Ceramics International 50 (2024) 37373–37378

Contents lists available at ScienceDirect

Ceramics International

journal homepage: www.elsevier.com/locate/ceramint

Cold sintering of proton-conducting half cells based on $BaZr_{0.7}Ce_{0.2}Y_{0.1}O_{3-\delta}$/NiO

Moritz Kindelmann [a,b,c,*], Martin Bram [c], Joachim Mayer [a,b], Olivier Guillon [c,d,**]

[a] Forschungszentrum Jülich GmbH Ernst Ruska-Centre for Microscopy and Spectroscopy with Electrons (ER-C), 52425 Jülich, Germany
[b] RWTH Aachen University, Central Facility for Electron Microscopy (GFE), 52074 Aachen, Germany
[c] Forschungszentrum Jülich GmbH, Institute of Energy and Climate Research, Materials Synthesis and Processing (IEK-1), 52425, Jülich, Germany
[d] Jülich Aachen Research Alliance, JARA-Energy, 52425, Jülich, Germany

ARTICLE INFO

Handling Editor: Dr P. Vincenzini

Keywords:
Cold sintering
Protonic ceramics
BZCY
Sintering
Solid oxide cell

ABSTRACT

Electrochemical devices based on proton conducting ceramic oxides have shown a high potential for conversion processes at intermediate temperatures. In these cells, perovskite ceramics like $BaZr_{0.7}Ce_{0.2}Y_{0.1}O_{3-\delta}$ (BZCY), which are based on the solid solution of $BaZrO_3$ and $BaCeO_3$ doped with Y, have proven to be a good compromise between chemical stability and proton conductivity. However, the refractory nature of this material system requires high sintering temperatures to enable dense ceramic membrane layers. Recently, a novel processing route, which applies the cold sintering process (CSP) as a pre-densification step has been developed allowing to lower the sintering temperatures while maintaining excellent electrochemical properties. In this study, we further improved this method by implementing a BZCY/NiO support layer for BZCY. After final thermal treatment under reducing conditions, a dense BZCY membrane supported by a porous BZCY/Ni electrode support resulted. We show that using powder processing techniques, it is possible to sinter thick layered structures, consisting of an almost dense, phase pure perovskite BZCY layer and a porous BZCY/NiO layer. Furthermore, the NiO phase was successfully reduced to Ni by an additional thermal treatment at 900 °C in Ar/H_2. The focus of this study was to generally prove the feasibility of applying co-cold sintering for the processing of layered ceramic architectures, which can be used – after further optimization of the processing – as electrode supported fuel or electrolysis cells.

1. Introduction

Protonic ceramics based on barium zirconate have a large potential for future energy conversion systems due to their reversible and robust performance at intermediate temperatures [1]. Recent developments have shown this potential for fuel and electrolyser cells [2–6] and membrane reactors [7–10]. Currently, most of high-performance proton conductors are based on a $BaZrO_3$ and $BaCeO_3$ solid solutions, additionally adding Y as an acceptor dopant (BZCY) for generating oxygen vacancies. This class of materials yields good proton conductivity as well as high chemical stability against CO_2 [11]. The implementation of oxygen vacancies is necessary to facilitate proton conduction through proton hopping by the Grotthuss mechanism. Therefore, atmospheric water has to be dissociated into oxygen vacancies following equation (1) [12,13].

$$H_2O + V_O^{\cdot\cdot} + O_O^x \rightarrow 2OH_O^{\cdot}$$

The major drawback of chemically stable Zr-rich compositions of BZCY is their refractory nature, which requires very high sintering temperatures around 1600 °C. Two measures are usually applied to improve the sintering behavior. On the one hand, transition metal oxides (e.g., NiO) are added as sintering aids. On the other hand, the desired BZCY phase is formed *in situ* during sintering, also known as solid state reactive sintering (SSRS). The combination of both measures decreases the overall processing temperatures to around 1500 °C [14–18]. However, the use of sintering aids is often coupled with performance losses caused by a decreased proton uptake capability due to lower effective acceptor concentrations [19,20]. Regardless of these recent improvements, the high processing temperatures of $BaZrO_3$ based proton conductors remains a major obstacle, motivating the development of new processing routes to reduce the overall sintering temperatures [21].

* Corresponding author. Forschungszentrum Jülich GmbH Ernst Ruska-Centre for Microscopy and Spectroscopy with Electrons (ER-C), 52425 Jülich, Germany.
** Corresponding author. Forschungszentrum Jülich GmbH, Institute of Energy and Climate Research, Materials Synthesis and Processing (IEK-1), 52425, Jülich, Germany.
E-mail addresses: m.kindelmann@fz-juelich.de (M. Kindelmann), o.guillon@fz-juelich.de (O. Guillon).

https://doi.org/10.1016/j.ceramint.2024.04.044
Received 20 February 2024; Received in revised form 27 March 2024; Accepted 3 April 2024
Available online 4 April 2024

A promising approach to lower the maximal processing temperatures of ceramic materials are innovative sintering techniques like the cold sintering process (CSP). In 2016, CSP was introduced by Randall et al. as a pressure and liquid assisted sintering technique, enabling almost full densification of a multitude of ceramic materials at significantly reduced sintering temperatures, usually below 400 °C [22]. Cold sintering makes it possible to combine materials that cannot be processed using conventional methods, like metals/ceramics and polymers/ceramics. This allowed to develop a novel processing route, called cold sintered co-fired ceramics (CSCC), which is mostly applied for multilayer capacitors [23,24].

Several mechanisms for the densification at such low temperatures are under discussion including a combination of pressure induced solution and re-precipitation at the particle surfaces [25,26] as well as plastic flow [27]. Even though some general observations have been described in literature, the cold sintering ability is very material specific. Recently, several authors achieved promising results when applying cold sintering for the densification of Y doped $BaZrO_3$ (BZY) [28,29], as well as different BZCY based ceramics [30–33].

To improve the electrochemical performance of ion conducting membranes, an obvious approach is to decrease the membrane thickness. To maintain sufficient mechanical stability, supporting the membrane by one of the electrodes resulting in a bi-layered cell architecture is an established solution in many electrochemical devices. In the present work, we adapted this concept for the manufacturing of an electrode supported proton conducting cell (PCC) aiming at demonstrating the processing of a dense BZCY membrane supported by a porous BZCY/Ni support at significantly reduced processing temperatures by taking advantage from the co-cold sintering of both layers as first processing step. Based on the achievements of our former studies [28,30,31], co-cold sintering of the BZCY and a BZCY/NiO layers was done at 350 °C using a uniaxial pressure of 400 MPa and deionized water as a sintering aid. Thermal post-treatment at 1300 °C in air as well as an additional treatment at 900 °C in Ar/H_2 to reduce NiO to metallic Ni have been conducted successfully on this structure proving the viability of co-cold sintering for the processing of layered protonic BZCY architectures. The focus of the present work was a fundamental feasibility study of this new processing method. Due to the still not optimized thickness of the BZCY membrane, electrochemical characterization of the layered cell architecture was out of scope and will be part of our future work.

2. Experimental methods

Ceramic powder with a nominal composition of $BaZr_{0.7}Ce_{0.2}Y_{0.1}O_{3-\delta}$ was used as starting material. The powder processing is based on a mixed oxide route which is optimized for pressure-less solid-state reactive sintering (SSRS) and therefore still contains 0.5 wt% NiO as a sintering aid [34]. The powder precursors ($BaCO_3$, Y_2O_3, ZrO_2, and CeO_2 (Sigma Aldrich, Germany) were dried, mixed, and pre-calcined at 1100 °C for 1 h. Afterward, NiO (Sigma Aldrich, Germany) was added as sintering aid, and the powders were wet milled for 24 h in isopropanol using zirconia ball and jar. For improving the cold sintering ability of the powder mixture, an additional calcination step at 1300 °C for 5 h was introduced [31]. After calcination, the powder was crushed and milled in ethanol for 30 min at 400 min^{-1} using a planetary ball mill (Retsch PM-400, Germany). Milling was done in a ZrO_2 milling jar adding 3 mm ZrO_2 balls. Finally, the calcined powders were dried at 80 °C for 24 h in air and sieved through a 100 μm sieve to remove larger agglomerates. The starting powder had an average particle size (d_{50}) of 600 nm and was softly agglomerated. The particle size distribution of the applied powder was determined using a LA950 laser granulometer (Horiba, Japan). The powders were measured in ethanol after 5 min of ultrasonic treatment.

All cold sintering experiments are carried out in a field-assisted sintering technology/spark plasma sintering machine (FAST/SPS, FCT Systeme HP-D5, Germany) using a metallic TZM die set-up (TZM = Mo-based alloy from Plansee SE, Austria) with a diameter of 12 mm. The inner surfaces of the pressing mold as well as the punches are covered with a thin graphite foil (d = 0,38 mm, Mersen, Germany) to facilitate sample removal after densification. In this study, a 50/50 wt% mixture of BZCY and NiO are used for the support layer 1.5 g of this powder mixture (corresponding to a layer thickness of 2 mm) were filled in the die. Then, 0.5 g of pure BZCY powder (estimated layer thickness of 700 μm) was placed on the top of support layer. Afterward, both layers were pre-compacted together with a pressure of 50 MPa. Then, 5 wt% deionized water was homogeneously added to the composite green body using a micropipette (Eppendorf, Germany). The bi-layered structure was densified at a sintering temperature of 350 °C, applying a uniaxial pressure of 400 MPa, a heating rate of 20 K/min, and a dwell time of 5 min. The temperature was monitored using a K-type thermocouple that is inserted into a hole in the TZM die. After cold sintering, all samples were subjected to thermal post-treatment (TPT) at 1300 °C for 10 h in air to reform the perovskite phase as described elsewhere [31,32]. Finally, the layered structure was thermally treated at 900 °C for 2h in reducing Ar/H_2 atmosphere to form a porous BZCY/Ni cermet composite layer. The porosity is formed due to the volume decrease related to the reduction of NiO to metallic Ni. The phase composition of the cold sintered bi-layered structure, the TPT samples and the reduced half-cell was measured by X-ray diffraction (XRD, Brucker D4 Endeavor, USA). Additionally, scanning electron microscopy (SEM) was applied to investigate the microstructure of the sintered samples in all three states of processing. Due to the water sensitivity and the submicron structure of cold sintered samples, fracture surfaces were characterized using a Zeiss Ultra 55 SEM (Zeiss, Germany). All other samples were embedded, metallographically polished and characterized using a FEI Phenom tabletop SEM (FEI, USA).

3. Results and discussion

In the following, the microstructural change of both layers after each processing step will be discussed. Firstly, Fig. 1a gives a schematic representation of the processing route described in this study. It consists of three major steps: (1, 2) powder wetting and cold sintering, (3) thermal post-treatment and (4) NiO reduction treatment. Details on the densification during cold sintering are given in Fig. 1b. The relative displacement during cold sintering as well as the chamber gas pressure are plotted over the sintering temperature. As the cold sintering experiment is conducted inside a FAST/SPS chamber in vacuum, an increase in chamber pressure can directly be associated to the evaporation of the liquid sintering aid. It is clearly observable that the water evaporation during the heating phase is coupled to the densification curve. The displacement curve is reaching a plateau when exceeding 250 °C, directly after the evaporation starts to decrease. After achieving the maximum cold sintering temperature of 350 °C, the bi-layered half-cell has reached its highest level of densification. After the dwell time, the temperature and pressure decrease lead to an elastic expansion of the tool setup and the sample, that can be observed as a decrease in relative displacement. As already analyzed and discussed in our previous studies [31,32], the cold sintering of BZCY under high mechanical pressure at such low temperatures is based on a pressure-assisted solution and re-precipitation mechanism, which is triggered by a partial decomposition of the Ce-rich BZCY phase. The microstructure after cold sintering at the interface between the BZCY/NiO support and the BZCY top layer is shown in Fig. 1c and d. The fracture surface indicates a good connection between both layers. The BZCY phase (indicated by the bright colored particles) reveals an extremely fine microstructure that did not show significant grain growth during the cold sintering process. The larger NiO particles are well-embedded in the BZCY/NiO support layer and seem to be less affected by the cold sintering process.

Even though densification could be achieved at low temperatures, the decomposition of the Ce-rich BZCY component – as expected from our former studies [30,31] – can be observed in XRD diffractograms

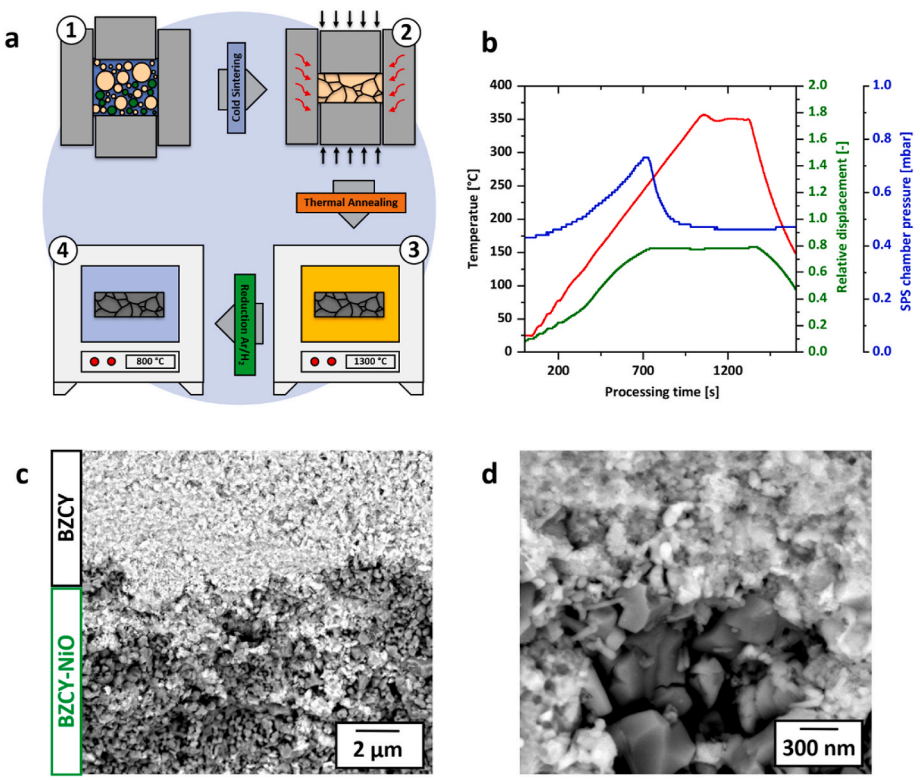

Fig. 1. Processing scheme and microstructure of the layered half-cell after cold sintering at 350 °C. (a) Schematic representation of the processing route: (1) Powder mixture with deionized water, (2) cold sintering process inside the FAST/SPS pressing tool, (3) Thermal post-treatment in air, (4) Reduction treatment in Ar/H_2 (b) Relative displacement (green curve), sintering temperature (red curve) and SPS chamber pressure (blue curve) visualizing the water evaporation curve during cold sintering (c, d) SEM images of the fracture surface at the interface between the BZCY/NiO and BZCY layers. (For interpretation of the references to color in this figure legend, the reader is referred to the Web version of this article.)

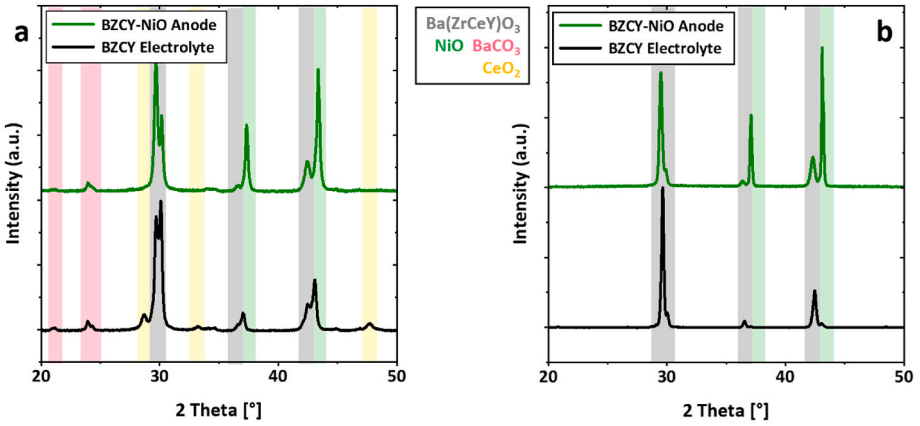

Fig. 2. Phase composition of the layered half-cell. (a) XRD diffractograms of both layers after cold sintering at 350 °C under 400 MPa for 5 min using deionized water. (b) XRD diffractograms of both layers after the TPT (1300 °C, 10 h, air).

(Fig. 2a). The formation of $BaCO_3$ as well as CeO_2 as decomposition products is especially pronounced in the BZCY layer (black diffractogram). On the composite electrode side, the XRD peaks of these side phases are less pronounced, possibly induced by the overall lower amount of BZCY (50 wt%) in this layer. The solution processes that activate the cold sintering are not expected to be affected by the addition of NiO to the composite layer. This kind of decomposition mechanism is on the one hand activating densification at low temperature but at the same time it is responsible for the formation of unstable secondary phases that prevent chemical stability in wet atmospheres [32] and deteriorates electrochemical performance drastically. Therefore, subsequent TPT is inevitable for cold sintered BZCY. Again, NiO seems to be not affected by the cold sintering process (see related peaks in the green diffractogram). The phase composition after a TPT at 1300 °C for 10 h is shown in Fig. 2b. All secondary phases formed during cold sintering (marked in yellow and red in Fig. 2a) are removed during the thermal treatment and the targeted BZCY phase is reformed. The diffractograms show only the expected peaks indicating the presence of single-phased BZCY and NiO.

Concerning the phase composition, the novel processing technology can be directly transferred from single bulk samples to layered structures. The implementation of 50 wt% of NiO as a second phase in the composite substrate layer did not interfere with the cold sintering and the reformation of the perovskite phase during TPT. To go a step further,

we did an additional thermal treatment of the TPT sample under reducing conditions to form a porous BZCY/Ni metal composite substrate approaching the cell architecture of an anode supported PCC. SEM images of the microstructure at substrate-membrane interface in different magnifications are shown in Fig. 3. The sample after TPT (Fig. 3 a, b) shows almost dense microstructures of both layers, with only a small amount of residual porosity (2.1 ± 0.9 % estimated by image analysis). The NiO second phase (dark grey) is well distributed, mainly because of good distribution of the fine BZCY starting powder around larger NiO particles. Nevertheless, the need of further improving the mixing of both phases is obvious. More important at this stage of development is the tight connection of both layers at the interface and also the interconnection of both phases within the BZCY/NiO composite is well pronounced. After the reduction treatment the composite layer reveals the aspired increase in porosity (ca. 30% using image analysis) enabling the gas transport if applied as PCC anode. The appearance of porosity is mainly caused by the volume decrease resulting from reduction of NiO to Ni metal. Even if mechanical tests are still pending, the porous structure that formed after reduction is stable and enables handling of the layered sample without special care. Furthermore, no delamination of BZCY membrane layer was observed. The present work is a general proof of concept that our novel, cold sintering-based processing technology is suitable to produce layered ceramics approaching the architecture of electrode supported electrochemically active cells. However, the current kind of processing prevents the manufacturing of thin layers with a thickness below 300 μm, which is necessarily required to produce well-performing electrode supported PCCs competitive to the state of the art [4,17,35,36]. Therefore, further optimization of the process is required to reduce the current layer thickness below 20 μm to allow an application of cold sintered samples as application-relevant proton conducting cell, e.g. by the implementation of tape cast layers as already demonstrated recently for YSZ/NiO-YSZ composites [37].

4. Conclusions

In this study, we demonstrated the potential of an additional cold sintering step for the densification of BZCY - BZCY/NiO bi-layered structures at clearly reduced sintering temperatures (here 1300 °C). Our results show that it is viable to sinter a dense BZCY membrane layer on top of a BZCY/NiO composite substrate approaching the cell architecture of an electrode supported proton conductor. Therefore, we cold sintered the bi-layered sample in a FAST/SPS device followed by a pressure-less thermal treatment at 1300 °C for 10h in air. A final thermal treatment at 900 °C under reducing Ar/H_2 conditions enabled the reduction of the NiO phase to metallic Ni resulting in the aspired porous BZCY/Ni metal composite substrate. The cold sintering step, which was conducted at 350 °C and 400 MPa using deionized water as sintering aid, enables a densification of both layers significantly above 80 %. This densification is mainly related to the densification of the fine grained BZCY phase and is based on a partial dissolution of the Ce-rich BZCY phase in the liquid sintering aid. Hereby, secondary phases ($Ba(OH)_2$, CeO_2 and $BaCO_3$) are formed making a subsequent thermal treatment necessary to reform the perovskite phase after cold sintering. This reformation is a basic requirement for an application in electrochemical devices. Furthermore, the treatment increased the stability of the sintered samples against wet atmospheres, e.g., for storage under ambient conditions. As investigated in more detail in our former works [31,32], thermal treatments at 1300 °C are sufficient to process stable BZCY - BZCY/NiO bi-layered structures. Furthermore, we demonstrated that is possible to reduce the NiO in the BZCY/NiO composite substrate by a thermal treatment in Ar/H_2 resulting in a porous BZCY/Ni metal composite substrate. Open porosity of the substrate is necessarily required for electrochemical applications to ensure gas transport in the substrate. Major drawbacks of the current kind of processing are the still high layer thickness, as well as the small sample size making our bi-layered BZCY – BZCY/Ni samples unsuitable for a reasonable electrochemical characterization. Therefore, further improvement of the processing

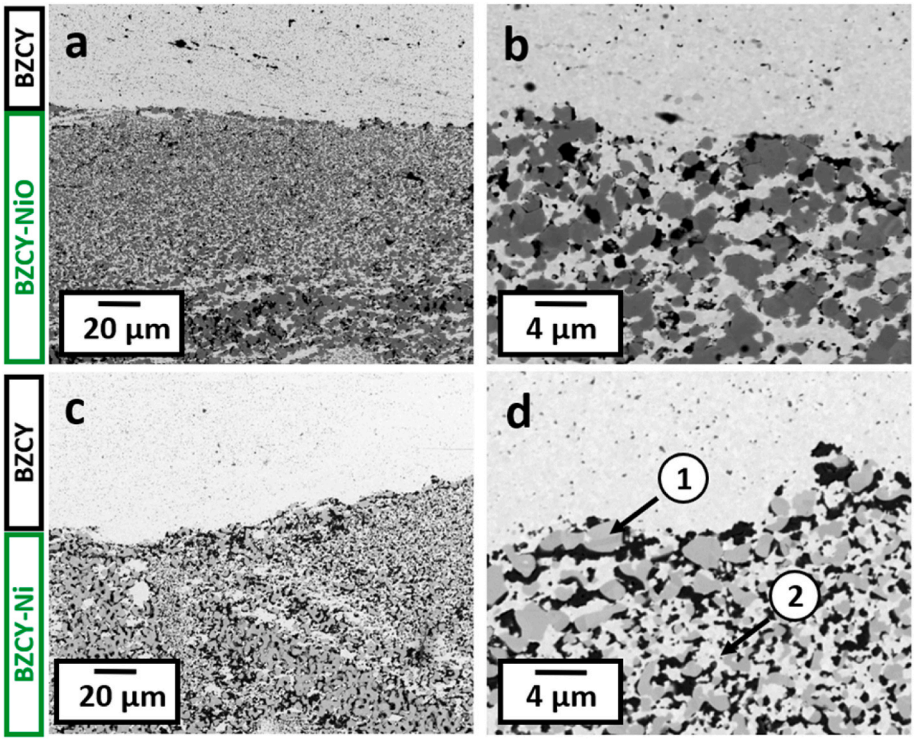

Fig. 3. Microstructure of a layered BZCY-BZCY/NiO half-cell after TPT and after subsequent reduction treatment. (a, b) Overview and detail SEM images of the interface between both layers after TPT (1300 °C, 10h, air) (c, d) Overview and detail image of the interface between both layers after a reduction treatment (900 °C, 2h, Ar/H2). Detail 1 shows the reduced Ni metal structure and detail 2 the remaining intact BZCY network.

technology, e.g., by implementing tape casting for the processing of thin layers, is necessarily required to also demonstrate an electrochemical performance competing or even exceeding the performance of conventionally processed electrode supported PCCs.

CRediT authorship contribution statement

Moritz Kindelmann: Conceptualization, Data curation, Investigation, Visualization, Writing – original draft, Writing – review & editing. **Martin Bram:** Project administration, Supervision, Writing – review & editing. **Joachim Mayer:** Funding acquisition, Project administration, Supervision, Writing – review & editing. **Olivier Guillon:** Funding acquisition, Supervision, Writing – review & editing.

Declaration of competing interest

The authors declare that they have no known competing financial interests or personal relationships that could have appeared to influence the work reported in this paper.

Acknowledgements

Dr. Doris Sebold is acknowledged for support with SEM imaging and Dr. Wendelin Deibert is acknowledged for providing the starting powders. M.K is acknowledging the financial support from the DFG in the project MA 1280/69-1.

References

[1] J.M. Serra, Electrifying chemistry with protonic cells, Nat. Energy 4 (2019) 178–179, https://doi.org/10.1038/s41560-019-0353-y.
[2] C. Duan, R.J. Kee, H. Zhu, C. Karakaya, Y. Chen, S. Ricote, A. Jarry, E.J. Crumlin, D. Hook, R. Braun, N.P. Sullivan, R. O'Hayre, Highly durable, coking and sulfur tolerant, fuel-flexible protonic ceramic fuel cells, Nature 557 (2018) 217–222, https://doi.org/10.1038/s41586-018-0082-6.
[3] S. Choi, C.J. Kucharczyk, Y. Liang, X. Zhang, I. Takeuchi, H. Il Ji, S.M. Haile, Exceptional power density and stability at intermediate temperatures in protonic ceramic fuel cells, Nat. Energy 3 (2018) 202–210, https://doi.org/10.1038/s41560-017-0085-9.
[4] F. Liu, H. Deng, D. Diercks, P. Kumar, M.H.A. Jabbar, C. Gumeci, Y. Furuya, N. Dale, T. Oku, M. Usuda, P. Kazempoor, L. Fang, D. Chen, B. Liu, C. Duan, Lowering the operating temperature of protonic ceramic electrochemical cells to <450 °C, Nat. Energy 8 (2023) 1145–1157, https://doi.org/10.1038/s41560-023-01350-4.
[5] L. Yang, S. Wang, K. Blinn, M. Liu, Z. Liu, Z. Cheng, M. Liu, Enhanced sulfur and coking Tolerance of a mixed ion conductor for SOFCs: BaZr0.1Ce0.7Y0.2–xYbxO3–d, Science 326 (2009) 126–129.
[6] E. Vøllestad, R. Strandbakke, M. Tarach, D. Catalán-Martínez, M.L. Fontaine, D. Beeaff, D.R. Clark, J.M. Serra, T. Norby, Mixed proton and electron conducting double perovskite anodes for stable and efficient tubular proton ceramic electrolysers, Nat. Mater. 18 (2019) 752–759, https://doi.org/10.1038/s41563-019-0388-2.
[7] C. Daniel, M.-F. Harald, B. Michael, Y.-T. Irene, B. Dustin, A. Simen, N. Kevin, A. Luca, P. Thijs, V.P. K, P.D. K, V.M. I, R.-B. Sonia, N. Truls, B.T. S, J.M. S, K. Christian, S. Aamodt, K. Nguyen, L. Ansaloni, T. Peters, P.K. Vestre, D.K. Pappas, J.M. Serra, C. Kjølseth, Single-step hydrogen production from NH3, CH4, and biogas in stacked proton ceramic reactors, Science 376 (2022) 390–393, https://doi.org/10.1126/science.abj3951.
[8] V. Kyriakou, I. Garagounis, A. Vourros, E. Vasileiou, A. Manerbino, W.G. Coors, M. Stoukides, Methane steam reforming at low temperatures in a BaZr0.7Ce0.2Y0.1O2.9 proton conducting membrane reactor, Appl. Catal. B Environ. 186 (2016) 1–9, https://doi.org/10.1016/j.apcatb.2015.12.039.
[9] V. Kyriakou, I. Garagounis, A. Vourros, E. Vasileiou, M. Stoukides, An electrochemical haber-bosch process, Joule 4 (2020) 142–158, https://doi.org/10.1016/j.joule.2019.10.006.
[10] H. Malerød-Fjeld, D. Clark, I. Yuste-Tirados, R. Zanón, D. Catalán-Martinez, D. Beeaff, S.H. Morejudo, P.K. Vestre, T. Norby, R. Haugsrud, J.M. Serra, C. Kjølseth, Thermo-electrochemical production of compressed hydrogen from methane with near-zero energy loss, Nat. Energy 2 (2017) 923–931, https://doi.org/10.1038/s41560-017-0029-4.
[11] K. Katahira, Y. Kohchi, T. Shimura, H. Iwahara, Protonic conduction in Zr-substituted BaCeO3, Solid State Ionics 138 (2000) 91–98, https://doi.org/10.1016/S0167-2738(00)00777-3.
[12] K.D. Kreuer, Aspects of the formation and mobility of protonic charge carriers and the stability of perovskite-type oxides, Solid State Ionics 125 (1999) 285–302, https://doi.org/10.1016/S0167-2738(99)00188-5.
[13] K.D. Kreuer, Proton-conducting oxides, Annu. Rev. Mater. Res. 33 (2003) 333–359, https://doi.org/10.1146/annurev.matsci.33.022802.091825.
[14] P. Babilo, S.M. Haile, Enhanced sintering of yttrium-doped barium zirconate by addition of ZnO, J. Am. Ceram. Soc. 88 (2005) 2362–2368, https://doi.org/10.1111/j.1551-2916.2005.00449.x.
[15] P. Babilo, T. Uda, S.M. Haile, Processing of yttrium-doped barium zirconate for high proton conductivity, J. Mater. Res. 22 (2007) 1322–1330, https://doi.org/10.1557/jmr.2007.0163.
[16] S. Ricote, N. Bonanos, Enhanced sintering and conductivity study of cobalt or nickel doped solid solution of barium cerate and zirconate, Solid State Ionics 181 (2010) 694–700, https://doi.org/10.1016/j.ssi.2010.04.007.
[17] S. Nikodemski, J. Tong, R. O'Hayre, Solid-state reactive sintering mechanism for proton conducting ceramics, Solid State Ionics 253 (2013) 201–210, https://doi.org/10.1016/j.ssi.2013.09.025.
[18] J. Tong, D. Clark, L. Bernau, M. Sanders, R. O'Hayre, Solid-state reactive sintering mechanism for large-grained yttrium-doped barium zirconate proton conducting ceramics, J. Mater. Chem. 20 (2010) 6333–6341, https://doi.org/10.1039/C0JM00381F.
[19] Y. Huang, R. Merkle, J. Maier, Effects of NiO addition on sintering and proton uptake of Ba(Zr,Ce,Y)O3−δ, J. Mater. Chem. A. 9 (2021) 14775–14785, https://doi.org/10.1039/d1ta02555d.
[20] A.M. Dayaghi, J.M. Polfus, R. Strandbakke, A. Pokle, L. Almar, S. Escolástico, E. Vøllestad, J.M. Serra, R. Haugsrud, T. Norby, Effects of sintering additives on defect chemistry and hydration of BaZr0.4Ce0.4(Y,Yb)0.2O3−δ proton conducting electrolytes, Solid State Ionics 401 (2023), https://doi.org/10.1016/j.ssi.2023.116355.
[21] J. Irvine, J.L.M. Rupp, G. Liu, X. Xu, S. Haile, X. Qian, A. Snyder, R. Freer, D. Ekren, S. Skinner, O. Celikbilek, S. Chen, S. Tao, T.H. Shin, R. O'Hayre, J. Huang, C. Duan, M. Papac, S. Li, V. Celorrio, A. Russell, B. Hayden, H. Nolan, X. Huang, G. Wang, I. Metcalfe, D. Neagu, S.G. Martín, Roadmap on inorganic perovskites for energy applications, JPhys Energy 3 (2021), https://doi.org/10.1088/2515-7655/abff18.
[22] J. Guo, H. Guo, A.L. Baker, M.T. Lanagan, E.R. Kupp, G.L. Messing, C.A. Randall, Cold sintering: a paradigm shift for processing and integration of ceramics, Angew Chem Int Ed Engl. 55 (2016) 11457–11461, https://doi.org/10.1002/anie.201605443.
[23] J. Guo, H. Guo, A.L. Baker, M.T. Lanagan, E.R. Kupp, G.L. Messing, C.A. Randall, J. Guo, C.A. Randall, D. Johnson, Cold sintering process: a novel technique for low-temperature ceramic processing of ferroelectrics, J. Am. Ceram. Soc. 55 (2016) 3489–3507, https://doi.org/10.1002/anie.201605443.
[24] D. Wang, D. Zhou, K. Song, A. Feteira, C.A. Randall, I.M. Reaney, Cold-sintered C0G multilayer ceramic capacitors, Adv. Electron. Mater. 5 (2019) 1900025, https://doi.org/10.1002/aelm.201900025.
[25] M.Y. Sengul, J. Guo, C.A. Randall, A.C.T. van Duin, Water-mediated surface diffusion mechanism enables the cold sintering process: a combined computational and experimental study, Angew. Chemie Int. Ed. 58 (2019) 12420–12424, https://doi.org/10.1002/anie.201904738.
[26] M. Haug, F. Bouville, J. Adrien, A. Bonnin, E. Maire, A.R. Studart, Multiscale deformation processes during cold sintering of nanovaterite compacts, Acta Mater. 189 (2020) 266–273, https://doi.org/10.1016/j.actamat.2020.02.054.
[27] J. Gonzalez-Julian, K. Neuhaus, M. Bernemann, J. da Silva, A. Laptev, M. Bram, O. Guillon, J. Pereira da Silva, A. Laptev, M. Bram, O. Guillon, Unveiling the mechanisms of cold sintering of ZnO at 250 °C by varying applied stress and characterizing grain boundaries by Kelvin Probe Force Microscopy, Acta Mater. 144 (2018) 116–128, https://doi.org/10.1016/j.actamat.2017.10.055.
[28] Z. Zhao, J. Gao, Y. Meng, K.S. Brinkman, J. Tong, Moderate temperature sintering of BaZr0.8Y0.2O3-δ protonic ceramics by A novel cold sintering pretreatment, Ceram. Int. 47 (2021) 11313–11319, https://doi.org/10.1016/j.ceramint.2020.12.257.
[29] M. Kindelmann, J.N. Ebert, D. Jennings, D. Sebold, W. Rheinheimer, M. Bram, J. Mayer, O. Guillon, Cold sintering of BaZr0.8Y0.2O3-δ ceramics: phase formation and grain boundary properties, J. Eur. Ceram. Soc. (2023), https://doi.org/10.1016/j.jeurceramsoc.2023.12.060.
[30] K. Thabet, E. Quarez, O. Joubert, A. Le Gal La Salle, Application of the cold sintering process to the electrolyte material BaCe0.8Zr0.1Y0.1O3-δ, J. Eur. Ceram. Soc. 40 (2020) 3445–3452, https://doi.org/10.1016/j.jeurceramsoc.2020.03.043.
[31] M. Kindelmann, J.N. Ebert, W.S. Scheld, W. Deibert, W.A. Meulenberg, W. Rheinheimer, M. Bram, J. Mayer, O. Guillon, Cold sintering of BaZr0.7Ce0.2Y0.1O3-δ ceramics by controlling the phase composition of the starting powders, Scr. Mater. 224 (2023) 115147, https://doi.org/10.1016/j.scriptamat.2022.115147.
[32] M. Kindelmann, S. Escolastico, L. Almar, A. Vayyala, D. Jennings, W. Deibert, W. A. Meulenberg, W. Rheinheimer, M. Bram, J.M. Serra, J. Mayer, O. Guillon, Highly conductive grain boundaries in cold-sintered barium zirconate-based proton conductors, J. Mater. Chem. A. 12 (2024) 3977–3988, https://doi.org/10.1039/D3TA07076J.
[33] P. Castellani, E. Quarez, C. Nicollet, O. Joubert, N. Gautier, P. Pers, G. Taillades, A. Le Gal, L. Salle, Cold-sintering and Li doped ZnO sintering aid for the densification of BaZr0.7Ce0.2Y0.1O3-δ proton conducting ceramics, Int. J. Hydrogen Energy (2023) 22–24.
[34] W. Deibert, M.E. Ivanova, Y. Huang, R. Merkle, J. Maier, W.A. Meulenberg, Fabrication of multi-layered structures for proton conducting ceramic cells, J. Mater. Chem. A. 3 (2021), https://doi.org/10.1039/d1ta05240c.

[35] F. Liu, D. Ding, C. Duan, Protonic Ceramic Electrochemical Cells for Synthesizing Sustainable Chemicals and Fuels, 2023 2206478, https://doi.org/10.1002/advs.202206478.
[36] W. Bian, W. Wu, B. Wang, W. Tang, M. Zhou, C. Jin, H. Ding, W. Fan, Y. Dong, J. Li, D. Ding, Revitalizing interface in protonic ceramic cells by acid etch, Nature 604 (2022) 479–485, https://doi.org/10.1038/s41586-022-04457-y.
[37] T. Ucun, M. Murutoglu, O. Ulasan, E. Demirkal, A. Buyukaksoy, Y.K. Tur, H. Yilmaz, Cold sintering of anode-supported 8YSZ/NiO-8YSZ bilayers for solid oxide fuel cells, ACS Appl. Energy Mater. (2021), https://doi.org/10.1021/acsaem.1c02483.